J Nanopart Res (2016) 18: 385
DOI 10.1007/s11051-016-3699-0

RESEARCH PAPER

The upconversion luminescence and magnetism in Yb^{3+}/Ho^{3+} co-doped LaF_3 nanocrystals for potential bimodal imaging

Sasidharanpillai S. Syamchand · Sony George

Received: 8 June 2016 / Accepted: 2 December 2016 / Published online: 17 December 2016

Abstract Biocompatible upconversion nanoparticles with multifunctional properties can serve as potential nanoprobes for multimodal imaging. Herein, we report an upconversion nanocrystal based on lanthanum fluoride which is developed to address the imaging modalities, upconversion luminescence imaging and magnetic resonance imaging (MRI). Lanthanide ions (Yb^{3+} and Ho^{3+}) doped LaF_3 nanocrystals (LaF_3 Yb^{3+}/Ho^{3+}) are fabricated through a rapid microwave-assisted synthesis. The hexagonal phase LaF_3 nanocrystals exhibit nearly spherical morphology with average diameter of 9.8 nm. The inductively coupled plasma mass spectrometry (ICP-MS) analysis estimated the doping concentration of Yb^{3+} and Ho^{3+} as 3.99 and 0.41%, respectively. The nanocrystals show upconversion luminescence when irradiated with near-infrared (NIR) photons of wavelength 980 nm. The emission spectrum consists of bands centred at 542, 645 and 658 nm. The stronger green emission at 542 nm and the weak red emissions at 645 and 658 nm are assigned to $^5S_2 \rightarrow {}^5I_8$ and $^5F_5 \rightarrow {}^5I_8$ transitions of Ho^{3+}, respectively. The pump power dependence of luminescence intensity confirmed the two-photon upconversion process. The nanocrystals exhibit paramagnetism due to the presence of lanthanide ion dopant Ho^{3+} and the magnetization is 19.81 emu/g at room temperature. The nanocrystals exhibit a longitudinal relaxivity (r_1) of 0.12 s^{-1} mM^{-1} and transverse relaxivity (r_2) of 28.18 s^{-1} mM^{-1}, which makes the system suitable for developing T2 MRI contrast agents based on holmium. The LaF_3 Yb^{3+}/Ho^{3+} nanocrystals are surface modified by PEGylation to improve biocompatibility and enhance further functionalisation. The PEGylated nanocrystals are found to be non-toxic up to 50 μg/mL for 48 h of incubation, which is confirmed by the MTT assay as well as morphological studies in HeLa cells. The upconversion luminescence and magnetism together with biocompatibility enables the adaptability of the present system as a nanoprobe for potential bimodal imaging.

Keywords Upconversion luminescence · LaF_3 nanocrystals · MRI · Bimodal imaging · Holmium · T2 contrast · Biomedical applications

Introduction

Lanthanide doped inorganic nanoparticles have emerged as a versatile platform for a range of potential optical as well as biomedical applications (Cooper et al. 2014). The biocompatible bifunctional nanoparticles with robust luminescence and profound magnetism can serve as potential nanoprobes for multimodal imaging (MMI), which combines two or more imaging modalities in a single system. MMI significantly improves

Electronic supplementary material The online version of this article (doi:10.1007/s11051-016-3699-0) contains supplementary material, which is available to authorized users.

S. S. Syamchand · S. George (✉)
Department of Chemistry, University of Kerala, Kariavattom Campus, Trivandrum, Kerala 695 581, India
e-mail: emailtosony@gmail.com

S. S. Syamchand
e-mail: syamchand.ss@gmail.com

the potential of non-invasive medical diagnosis by providing synergistic advantages over any single imaging modality and have advantages like high spatial resolution and soft tissue contrast (Lee et al. 2014; Jennings and Long 2009). Lanthanide based upconversion (UC) nanoparticles are promising candidates for MMI and many of such systems have been reported (DaCosta et al. 2014; Wu et al. 2015; Mader et al. 2010). They are preferred due to high resolution and penetration depth as well as lack of auto fluorescence and photo damage. The UC is a nonlinear optical phenomenon in which two or more low energy photons in the near-infrared (NIR) region converted into a high energy photon in UV, visible or NIR region. Lanthanide UC nanostructures generally comprised of an inorganic host matrix and lanthanide ion dopants. The host matrices and the dopants are the key factors that determine UC luminescence efficiency. Dopants (sensitizers and activators) provide a luminescence centre and the host matrices supply a platform for energy transfer between the dopants (Chen et al. 2016; Boyer et al. 2007). The phenomenon of UC has been explored in various nanosized matrices and an ideal host matrix should have low lattice phonon energies as well as chemical stability. Host matrices with minimum phonon energies have maximum radiative emission possibility and fluoride host materials are popular choices for developing UC nanostructures (Zhou et al. 2015; Naccache et al. 2015).

Lanthanum fluoride is associated with low phonon energy of 350 cm^{-1} (Zhang et al. 2011). This low phonon energy together with thermal stability and the capability to incorporate different lanthanide ion dopants makes LaF_3 as an ideal host material for UC luminescence (Phaomei and Singh 2013). Among the lanthanide ion dopants, Er^{3+}, Tm^{3+} and Ho^{3+} are often selected as activators due to their ladder-like energy levels. Yb^{3+} ion, owing to its large absorption cross section and favourable energy levels can act as a common sensitizer to enhance the UC emission (Haase and Schafer 2011). Here, LaF_3 is selected as the host matrix and lanthanide ions (Yb^{3+} and Ho^{3+}) as selected dopants to develop UC nanocrystals. Yb^{3+}/Ho^{3+} pair is selected in order to explore the strong paramagnetic behaviour of Ho^{3+}, which enables the applicability of the obtained UC system in developing contrast agents (CAs) for magnetic resonance imaging (MRI). Biocompatible and paramagnetic nanoparticles can serve as positive (T1) or negative (T2) CAs, depending on whether they give rise to a brightening or a darkening effect on the MR image. The commonly used CAs (Gd-complexes as T1 CAs and iron oxide as T2 CAs) are suitable only at lower magnetic field strengths less than 3 T and are inefficient at higher field strengths greater than 7 T. This is because Gd-complexes have reduced T1 relaxivity at field strengths above 3 T, and super paramagnetic iron oxide (SPIO) reaches its saturation magnetization over 1.5 T. The MR imaging at high field strengths can offer better imaging performance compared to conventional clinical scans at lower field of 1.5 T. But the T1 relaxivity (positive contrast) typically decreases with increasing field while T2 relaxivity becomes more efficient. In this circumstance, the T2 CAs based on Ho and Dy are significant due to their remarkable performance under high magnetic field (Das et al. 2012). Moreover, it has been observed that Ho^{3+} ion can attenuate X-rays and this peculiarity can be explored in developing contrast agents for computer tomography (CT) imaging, but high concentration requirement limits this possibility. In this context, our aim is to explore the magnetism of Ho^{3+} to develop T2 MR contrast agents.

The present study aimed at the development of bifunctional nanocrystals based on LaF_3 with UC luminescence and magnetism (LaF_3 Yb^{3+}/Ho^{3+}). The said system can be explored as nanoprobes for potential bimodal imaging, for application in UC luminescence imaging and MRI. The LaF_3: Yb^{3+}/Ho^{3+} nanocrystals fabricated through a microwave-assisted synthetic route are subjected to PEGylation to improve the biocompatibility and to enhance further functionalisation.

Experimental

Materials

Lanthanum nitrate ($La(NO_3)_3.6H_2O$, 99%) and Holmium chloride ($HoCl_3.6H_2O$, 99.9%) were purchased from Alfa Aesar. Ytterbium acetate ($Yb(OAc)_3.4H_2O$, 99.9%) was purchased from Sigma-Aldrich. Ammonium fluoride (NH_4F) and poly ethylene glycol (PEG, mean MW = 4000) were obtained from MERCK. All chemicals were used as received without further purification. Deionised water was used in the experiments throughout.

Microwave-assisted synthesis of LaF_3 Yb^{3+}/Ho^{3+} nanocrystals

The nanocrystals were synthesised by a microwave-assisted synthesis and the protocol adopted here is a duly modified

reported procedure (Khandpekar and Gaurkhede 2014). In a typical method, 10 mL of 0.2 M La $(NO_3)_3.6H_2O$ (2 mmol) is taken in a 100 mL beaker. About 3.8 mg of $HoCl_3.6H_2O$ (0.01 mmol) and 42.2 mg of Yb $(OAc)_3.4H_2O$ (0.1 mmol) were added to the solution and magnetically stirred for 5 min. A funnel with stopper is placed above the beaker and 10 mL of 0.6 M NH_4F (6 mmol) solution is then added dropwise through the funnel by keeping the whole assembly inside a conventional microwave oven and irradiation is performed at lower power range for 30 min (in an on–off mode set at 30 s). The doped LaF_3 nanocrystals thus obtained started to settle down and heating is continued to obtain ultrafine dried NPs. The particles were washed three times with deionised water and finally dried in the MW oven for about 15 min.

PEGylation of LaF_3 Yb^{3+}/Ho^{3+} nanocrystals

LaF_3: Yb^{3+}/Ho^{3+} nanocrystals were surface modified by PEGylation. In a typical procedure 75 mg of the nanocrystals were added to a solution of 10 mL deionised water and 50 mg PEG in a 50 mL beaker. The mixture is magnetically stirred well for 3 h. The obtained PEGylated nanocrystals were centrifuged, washed and dried.

Particle characterisation

Crystallinity of LaF_3 Yb^{3+}/Ho^{3+} nanocrystals was tested by Powder X-ray diffraction (XRD) using a Bruker AXS D8 Advance X-ray powder diffractometer and the source of X-ray used is CuKα radiation (λ = 1.5406 Å). Material composition was tested by energy dispersive X-ray spectrum (EDX), recorded by using JEOL Model JED-2300 spectrometer. Scanning electron microscopy (SEM) images were taken using JEOL Model JSM-6390 LV scanning electron microscope. Atomic force microscopy (AFM) images were taken by using a Bruker Dimension Edge atomic force microscope. High resolution transmission electron microscope (HR-TEM) images were acquired with a FEI Tecnai T30 transmission electron microscope, operating at 300 kV of acceleration voltage. Dynamic light scattering (DLS) analysis and zeta potential measurements were performed by using Horiba SZ-100 Zetasizer. The upconversion (UC) emission spectra of the nanocrystals were recorded using FLS920P Edinburgh Analytical instrument equipped with an external 980 nm diode laser as the excitation source. The magnetization (M-H curve) was measured at room temperature using a Lakeshore 7410 vibrating sample magnetometer. Fourier transform infrared (FTIR) spectra were recorded with a Shimadzu IR Prestige 21 spectrometer and the scanning range is from 400 to 4000 cm^{-1}.

Inductively coupled plasma mass spectrometry

The doping concentrations of lanthanide ion dopants Yb^{3+} and Ho^{3+} in LaF_3 Yb^{3+}/Ho^{3+} nanocrystals were estimated by inductively coupled plasma mass spectrometry (ICP-MS) using Thermo Scientific ICAP Qc. The external calibration was conducted using standard certified multi element solution (MERCK). The ion optics was tuned using Thermo scientific Tune-B ICAP-Q solution in standard mode and KED mode. The said nanocrystals were microwave digested (Anton Paar, Multiwave 3000) in ultrapure aquaregia prior to the analysis. The digested sample is diluted with Milli-Q water and analysis is performed at an operating plasma power of 1550 W.

r_1 and r_2 relaxivity measurements

The T_1 and T_2 relaxation times of LaF_3 Yb^{3+}/Ho^{3+} nanocrystals were measured using BrukerAvans 500 MHz NMR spectrometer. The measurements were carried out at 25 °C in spin echo method with time to echo (TE) = 9 ms, and the applied magnetic field strength is 11.7 T. A series of five aqueous solutions with different concentrations (1, 0.5, 0.125, 0.0625 mM of Ho^{3+}) were prepared. $T_1$and T_2 relaxation times were measured with these solutions, and the relaxivities (r_1 and r_2) were calculated from the slopes in the plots of $1/T_1$ and $1/T_2$ against Ho^{3+} concentration.

Cell culture and cytotoxicity assay

Human cervical cancer cells (HeLa) were procured from NCCS, Pune, India. The cells were grown in Dulbecco's Modified Eagle Medium (DMEM) supplemented with 10% foetal bovine serum (FBS) 1% penicillin and streptomycin solution at 37 °C and 5% CO_2. The cells were subcultured at regular intervals (70–80% confluency) and the doubling time was found to be 24 h. The in vitro cell viability was measured using 3-(4, 5-dimethylthiazol-2yl)-2, 5 diphenyl-tetrazolium bromide (MTT) assay in HeLa cells, which was maintained in culture in DMEM under standard conditions. In a

typical procedure, HeLa were seeded in 96-well microplate (1×10^4cells/well) and allowed to attach. After that, the medium containing different concentrations (10, 20, 30, 40 and 50 μg/mL) PEGylated nanocrystals were added and incubated for different time intervals (4, 8, 12, 24 and 48 h). After incubation, the medium was removed and supplemented with a fresh medium containing MTT and incubated for 4 h. After removing the medium containing MTT, the formazan crystals formed were completely dissolved in DMSO solvent and the absorbance was measured at 570 nm. Phase contrast microscopy is employed to study the effect of nanocrystals on the morphology of the HeLa cells.

Results and discussion

Synthesis of LaF_3 Yb^{3+}/Ho^{3+} nanocrystals

Several methods are employed for the fabrication of doped LaF_3 nanocrystals and the common methods are co-precipitation (Stouwdam and vanVeggel 2002; Liu et al. 2008; Singh et al. 2013) and hydrothermal synthesis (Hu et al. 2008; Zhang et al. 2005). Lanthanum fluoride is associated with a small solubility product constant (K_{sp}) of 2.0×10^{-19} at 25 °C, and it implies a rapid reaction between La^{3+} and $F^-$to produce the precipitate of LaF_3. Therefore, it is difficult to control the morphology and size of LaF_3 nanocrystals during the wet chemical synthesis (Zhu et al. 2007). The microwave (MW) assisted synthesis can offer better control over size as well as morphology, and in the present study nanocrystals were prepared through a MW assisted route. The method employed is a reported protocol with adequate modification (Khandpekar and Gaurkhede 2014). The MW irradiation time, stoichiometric ratio of the reactants and dropwise addition of the fluoride precursor (NH_4F) to the lanthanum salt solution ($La(NO_3)_3$) during irradiation are the key factors to obtain LaF_3 nanocrystals of uniform morphology. The dropwise addition of fluoride during irradiation is carried out by using a funnel with stopper over the beaker containing La^{3+}, which is placed inside the MW oven during irradiation. The irradiation time is optimised at 30 min and low power range is preferred to avoid spill-off of solution. The lanthanum salt solution ($La(NO_3)_3$) is thoroughly mixed with the lanthanide ion dopants (Yb^{3+} and Ho^{3+}) prior to reaction with fluoride precursor and consequent MW irradiation. It enabled their successful doping in the nanocrystals, which confirmed by further analysis.

Crystal structure, shape and size of LaF_3 Yb^{3+}/Ho^{3+} nanocrystals

The functional properties like magnetism and luminescence of the nanoparticles are invariably related to the crystallographic parameters, shape as well as size. The crystallinity of the as prepared nanocrystals was tested by the X-ray powder diffraction (XRD) analysis. The XRD pattern of perfectly dried and finely powdered nanocrystals is shown in Fig. 1a. The peak positions and intensities agree well with the data reported in JCPDS card (32–0483) of pure hexagonal phase LaF_3 crystals (Zhu et al. 2007). As per the Scherrer formula, size of nanoparticles is inversely proportional to the width of XRD diffraction peaks. Thus, the diffraction peaks with large width (Fig. 1a) is an indication of the nanosize of the as prepared particles (Srinivasan et al. 2014). The impurity peaks such as that of oxides (Yb_2O_3 or Ho_2O_3) are totally absent in the XRD pattern, which led to the conclusion that the dopants were incorporated into the lattice of nanocrystalline LaF_3. The energy dispersive X-ray (EDX) analysis is performed to check the chemical purity and elemental compositions of the nanocrystals. The EDX spectrum of the LaF_3 are synthesised by adding the dopants 0.1 mmol Yb^{3+} and 0.01 mmol Ho^{3+} is shown in Fig. 1b. The spectrum displays elemental peaks related to La, F, Yb and Ho. This result confirms the detectable levels of lanthanide ion dopants within LaF_3 matrix. The concentration of the dopants in the nanocrystals were estimated by ICP-MS analysis, and the results shown that 3.99% of Yb^{3+} and 0.41% of Ho^{3+} are present in the as prepared LaF_3 nanocrystals. Further studies were conducted based on this concentration.

Morphology and size of the LaF_3 Yb^{3+}/Ho^{3+} nanocrystals were analysed by AFM, SEM and HR-TEM. The AFM phase image of the nanocrystals, taken in the tapping mode and SEM image of the finely powdered nanocrystals are provided in the electronic supplementary material (ESM) (Fig. S1 and S2). The AFM and SEM analysis proved the existence of nearly spherical particles in the nano regime. The size and morphology of the nanocrystals were confirmed by HR-TEM analysis. Figure 2a–c represent the HR-TEM images and the analysis reveals the existence of nearly spherical nanocrystals with an average diameter of

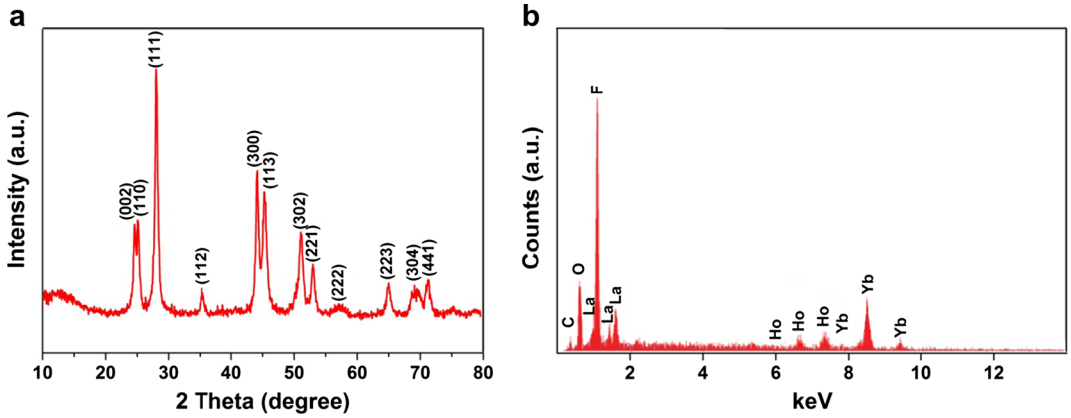

Fig. 1 **a** X-ray diffraction spectrum and **b** energy dispersive X-ray analysis spectrum of LaF_3 Yb^{3+}/Ho^{3+} nanocrystals

9.8 nm. The selective area electron diffraction (SAED) pattern (Fig. 2d) clearly depicted the diffraction rings corresponds to (002), (111), (300) and (113) planes of LaF_3 nanocrystals and it suggests the random alignment of LaF_3 nanocrystals (Gayathri et al. 2015). The as prepared nanocrystals exhibit a stable zeta potential value of −32 mV (Fig. S3, ESM). Dynamic light scattering (DLS) analysis was performed to evaluate the hydrodynamic size distribution of the nanocrystals and results obtained are shown in Fig. S4, ESM. The DLS data reveals that most of the nanoparticles are in the hydrodynamic size range of 28–31 nm.

Upconversion luminescence in LaF_3 Yb^{3+}/Ho^{3+} nanocrystals

LaF_3 Yb^{3+}/Ho^{3+} nanocrystals exhibit UC luminescence when excited with NIR photons of 980 nm, using diode laser as the excitation source and the UC emission spectra is shown in Fig. 3a. The nanocrystals show

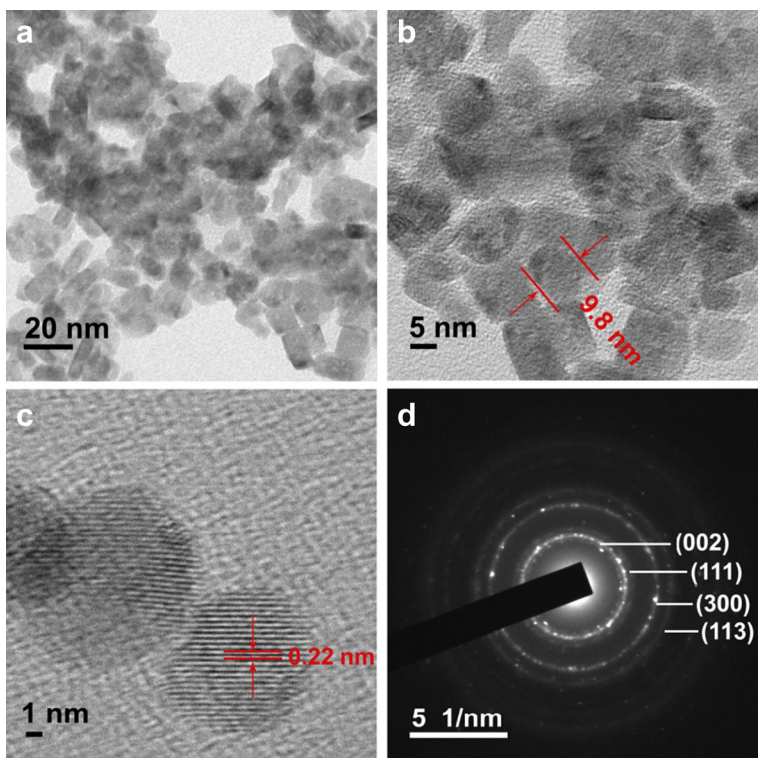

Fig. 2 **a**–**c** HR-TEM images and **d** SAED pattern LaF_3 Yb^{3+}/Ho^{3+} nanocrystals

emission bands centred at 542, 645 and 658 nm. The spectrum obtained is comparable in shape as well as in peak positions with previous reports (Liu and Chen 2007; Huang 2016). The stronger green emission at 542 nm corresponds to $^5S_2 \rightarrow {}^5I_8$ transition of Ho^{3+} and the weak red emissions at 645 and 658 nm were assigned to $^5F_5 \rightarrow {}^5I_8$ transition of Ho^{3+} (Liu and Chen 2007). It is well established that the UC emission intensity I_{up} depends upon the exciting power as per the relation $I_{up} \propto (I_{ex})^n$, where n is the number of photons involved in the UC process. The pump power dependence of UC luminescence intensity is tested to find out the number of photons involved in UC process. Figure 3b represents the log-log plots of pump power dependence of the green and red emissions. The slopes (values of n) are fitted as 1.86, 1.58 and 1.64 for the emissions at 542, 645 and 658 nm respectively. These values of n confirm that two photons process mainly contributes to the green and red emissions in the said nanocrystals. The pump power dependence of UC luminescence intensity is also tested at low laser powers up to 100 mW and the results (Fig. S5, ESM) revealed that the UC emission is visible even at low laser powers in the range of 100 mW. The UC emission intensity in the present system is comparable with other UC nanomaterials with similar dopants (Yu et al. 2014).

The population process and UC emissions can be explained by considering the simplified energy level diagrams of Ho^{3+} and Yb^{3+} ions (Fig. 4). Yb^{3+} ion serves as an effective sensitizer owing to its large absorption cross section and high doping concentration (3.99%) compared to Ho^{3+} (0.41%) (Yu et al. 2014). As a result of 980 nm NIR irradiation, the Yb^{3+} ions are

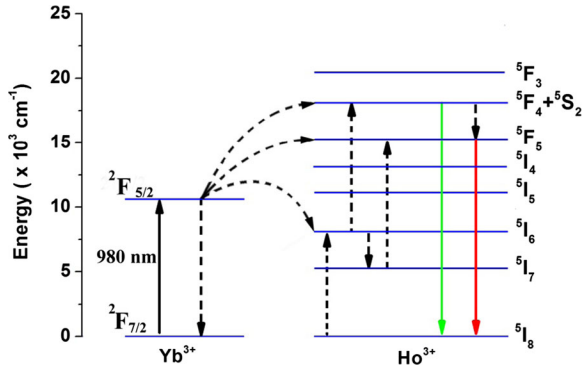

Fig. 4 Simplified energy level diagrams of Ho^{3+} and Yb^{3+} ions and possible UC mechanisms

excited from $^2F_{7/2}$ to $^2F_{5/2}$ level and transfer the absorbed energy to nearby Ho^{3+} ions (activator). Consequently, the Ho^{3+} ions are excited to the $^5I_6$ level by energy transfer process (ET) as $^2F_{5/2}(Yb^{3+}) + {}^5I_8(Ho^{3+}) \rightarrow {}^2F_{7/2}(Yb^{3+}) + {}^5I_6(Ho^{3+})$. As a result of excited state absorption (ESA) or a possible second ET process, Ho^{3+} ions in $^5I_6$ levels are excited directly to $(^5F_4 + {}^5S_2)$ level as $^2F_{5/2}(Yb^{3+}) + {}^5I_6(Ho^{3+}) \rightarrow {}^2F_{7/2}(Yb^{3+}) + {}^5F_4 / {}^5S_2(Ho^{3+})$. The radiative transfer from the present level to $^5I_8$ ground level results in green emission centred at 542 nm. Moreover, through a non-radiative process, Ho^{3+} ions in the $^5I_6$ level drops to $^5I_7$ level and further excited to $^5F_5$ level by another ET process as $^2F_{5/2}(Yb^{3+}) + {}^5I_7(Ho^{3+}) \rightarrow {}^2F_{7/2}(Yb^{3+}) + {}^5I_5(Ho^{3+})$. Another possibility to populate $^5I_5$ level of Ho^{3+} is the multiphonon relaxation process of Ho^{3+} from $(^5F_4 + {}^5S_2)$ level to $^5I_5$ level. The radiative transfer from $^5F_5$ level to $^5I_8$ ground level results in red emissions centred at 645 and 658 nm. However, a three photon

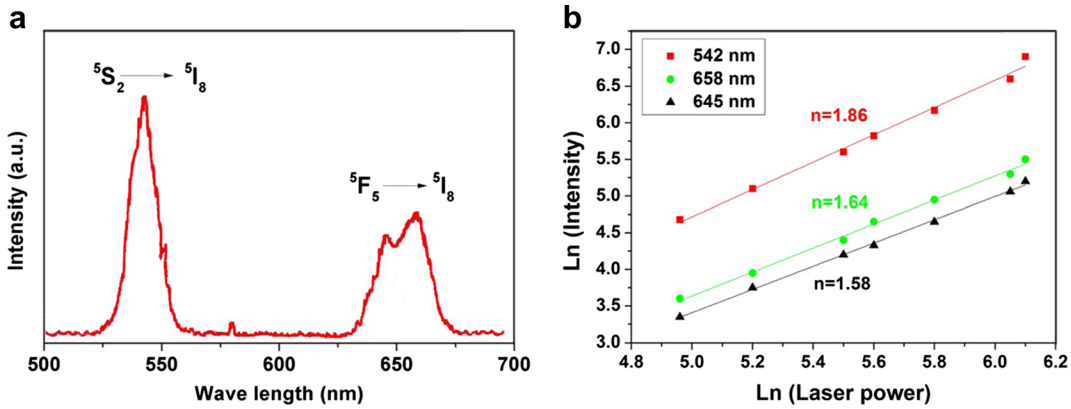

Fig. 3 **a** Upconversion emission spectra and **b** log-log plots of pump power dependence of the green and red emissions of LaF_3 Yb^{3+}/Ho^{3+} nanocrystals

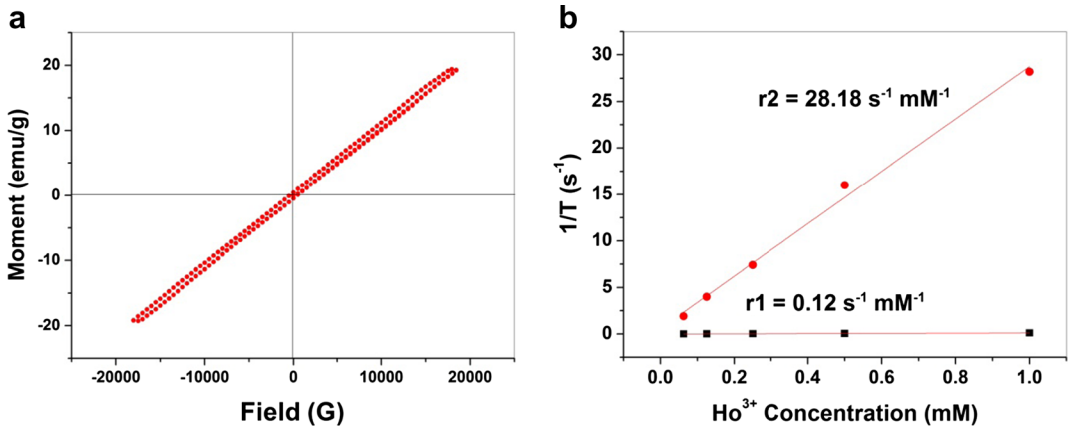

Fig. 5 **a** The room temperature magnetisation against applied magnetic field (M–H) curve and **b** plots of $1/T_1$ and $1/T_2$ inverse relaxation times of LaF_3 Yb^{3+}/Ho^{3+} nanocrystals

process can generate a blue emission due to $^5F_3 \rightarrow {}^5I_8$ transition of Ho^{3+} (Huang 2016; Dong et al. 2015).

Magnetic property and relaxivities

The presence of highly paramagnetic lanthanide ion dopant, Ho^{3+} ion endowed magnetism to LaF_3 Yb^{3+}/Ho^{3+} nanocrystals. The magnetic properties of the said nanocrystals are explored by VSM analysis. Figure 5a represents the room temperature magnetisation against applied field (M-H) curve of the nanocrystals that contain 0.41% Ho^{3+} and 3.99% Yb^{3+}. The M–H curve clearly indicates the paramagnetic nature of the nanocrystals and the magnetization value is 19.81 emu/g. The Dy^{3+} and Ho^{3+} by virtue of their very short electronic relaxation time due to their highly anisotropic ground state can perform as efficient T2 contrast agents in intermediate and high magnetic field strengths. Several reports are available on T2 contrast agents that are developed from paramagnetic lanthanide ions such as Dy, Ho, Tb and Er (Norek and Peters 2011; Vuong et al. 2012; Kattel et al. 2011). The water proton relaxivity is a key factor which permits the utility of the nanocrystals as contrast agents. In order to explore the present system as new holmium based T2 MRI contrast agent, their water proton relaxivities were measured. The longitudinal (T_1) and transverse (T_2) relaxation times are measured by using standard solutions of the nanocrystals with different concentrations (1, 0.5, 0.125, 0.0625 mM) of Ho^{3+}. These solutions are obtained by dilution from a mother solution of the said nanocrystal, which contain 0.41% of Ho^{3+}. The inverse of relaxation times ($1/T_1$) and $1/T_2$) are plotted against Ho^{3+}concentration and the graphs obtained are shown in Fig. 5b. The slope of the curves gives a longitudinal relaxivity (r_1) of 0.12 s^{-1} mM^{-1} and transverse relaxivity (r_2) of 28.18 s^{-1} mM^{-1}. The high r_2 relaxivity suggests the adaptability of the nanocrystals as holmium based T2 MRI contrast agent.

Surface modification of LaF_3 Yb^{3+}/Ho^{3+} nanocrystals

In order to explore in bioanalytical applications, the surface properties of the nanocrystals must be well designed to permit both the formation of a stable

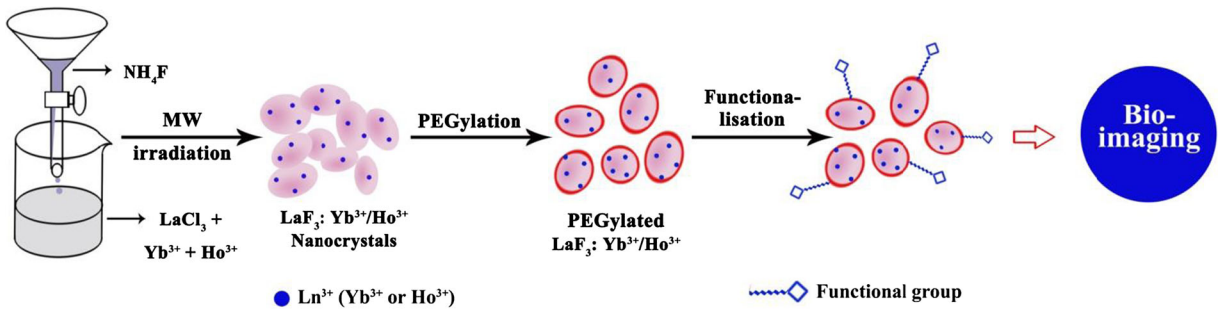

Scheme 1 Schematic illustration of the synthesis and PEGylation of LaF_3 Yb^{3+}/Ho^{3+} nanocrystals

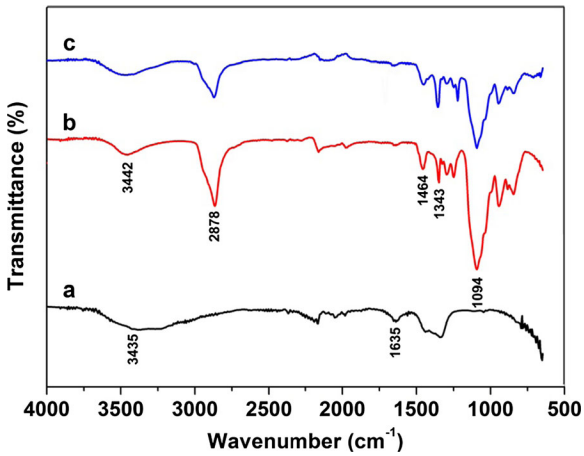

Fig. 6 FTIR spectra **a** LaF_3 Yb^{3+}/Ho^{3+} nanocrystals, **b** pure PEG and **c** PEGylated LaF_3 Yb^{3+}/Ho^{3+} nanocrystals

colloidal dispersion and the ability to conjugate biomolecules or other ligands on the surface (Sedlmeier and Gorris 2015). LaF_3: Yb^{3+}/Ho^{3+} nanocrystals exhibit UC luminescence and substantial magnetic properties, which make them feasible in bioimaging. The said nanocrystals are surface modified by coating with PEG to ensure enhanced biocompatibility and adaptability in bioimaging. The MW synthesis and PEGylation of the nanocrystals are illustrated in Scheme 1. PEG provide a green reaction media as well as many advantages for biological applications like enhanced biocompatibility, minimal non-specific interaction with other proteins and protection of the nanomaterials from immune system while used in vivo (Chen et al. 2005; Jokerst et al. 2011; Otsuka et al. 2003). PEGylation with functionalised PEG can bring about the generation of terminal functional groups in nanocrystals, and it enables the conjugation of other biomolecules, targeting ligands or reporter moieties. In the present system, the PEGylation happens through physical interaction between LaF_3 nanocrystals and PEG.

FTIR spectra are used to confirm the surface modification of the nanocrystals through PEGylation. Figure 6a shows the FTIR spectrum of bare LaF_3 Yb^{3+}/Ho^{3+} nanocrystals. As the nanocrystals are synthesised in aqueous medium, their surface may be covered by a large number of O–H groups either chemically bonded or adsorbed. The absorption band at around 3435 and 1635 cm^{-1} are due to the O–H stretching and bending vibrations (Wang et al. 2006). Figure 6b shows the FTIR spectrum of pure PEG and the band at 1094 and 3442 cm^{-1} is due to O–H stretching of alcohol and water, respectively. The bands at 1343 and 1464 cm^{-1} are due to C–H bending. The band at 2878 cm^{-1} is due to C–H stretching (Shameli et al. 2012). Figure 6c shows the FTIR spectrum of PEGylated LaF_3 Yb^{3+}/Ho^{3+} nanocrystals. From the spectra, it is clear that the functional peaks of PEG remain intact during PEGylation of the nanocrystals, which implies the lack of chemical bond formation between PEG and LaF_3 as well as successful surface coating through PEGylation.

Cytotoxicity of PEGylated nanocrystals

For the adaptability of the nanoparticles in biomedical applications, biocompatibility must be ensured. The cytotoxicity of the PEGylated nanocrystals is tested by MTT assay in HeLa cells and the results are shown in Fig. 7a. The assay confirmed the non-toxicity of the nanocrystals up to 50 μg/mL for 48 h of incubation.

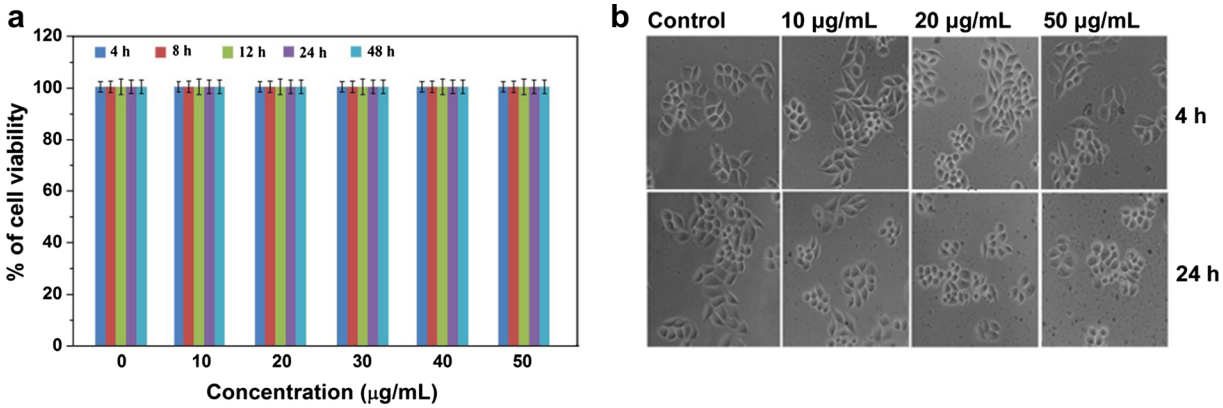

Fig. 7 **a** MTT assay showing the non-toxicity of PEGylated LaF_3 Yb^{3+}/Ho^{3+} nanocrystals in HeLa cells and **b** phase contrast microscopic images showing the effect nanocrystals on cell morphology of HeLa cells

The effect of PEGylated nanocrystals on the morphology of the HeLa cells were tested by phase contrast microscopy at different concentrations (10, 20 and 50 μg/mL) for different incubation times (4 and 24 h) and the obtained phase contrast microscopic images are shown in Fig. 7b. The results revealed that up to 50 μg/mL concentration for 24 h of incubation, the morphology of the cells remains the same. On the basis of MTT assay and cell morphological analysis, it can be concluded that the PEGylated nanocrystals are biocompatible and non-toxic to live cells and hence promising candidates for in vivo bioimaging applications.

Conclusions

In summary, we prepared lanthanide ions (Yb^{3+}andHo^{3+}) doped LaF_3 nanocrystals (LaF_3 Yb^{3+}/Ho^{3+}) with UC luminescent and magnetic properties through a rapid microwave-assisted synthesis. The particles were characterised by different methods and dopant concentrations estimated. The obtained nearly spherical nanocrystals exhibited functional properties due to lanthanide ion dopants. The nanocrystals showed distinct UC luminescence during NIR excitation at 980 nm, and the emission spectrum contain bands centred at 542(green emission), 645 and 658 nm (red emissions). The pump power dependence on UC emission intensity confirmed the two-photon UC process. The magnetic property of the nanocrystals is explored and the paramagnetism is endowed by the lanthanide ion, Ho^{3+}. The relaxivity measurements (r_1 and r_2) of the nanocrystals revealed a substantial r_2 relaxivity of 28.18 s^{-1} mM^{-1}. The LaF_3 Yb^{3+}/Ho^{3+} nanocrystals are PEGylated for improved biocompatibility and ease of further conjugation. The PEGylated nanocrystals were analysed for toxicity through MTT assay, and the effects of nanocrystals on the morphology of HeLa cells were tested. The results showed the non-toxicity of the nanocrystals up to 50 μg/mL for 48 h of incubation. The UC luminescence can be explored for UC luminescence imaging and the substantial r_2 relaxivity can be utilised in developing Ho based T2 MR contrast agents. Thus, the present system can serve as potential nanoprobes for bimodal imaging.

Acknowledgements The authors thank the Director, National Centre for Ultrafast Process (NCUP, University of Madras), Director, CSIR-NIIST (Thiruvananthapuram), Head, SAIF-IIT Madras, Director, IISER (Thiruvananthapuram), Director, SAIF-STIC-CUSAT (Kochi) and the Head, Department of Chemistry, University of Kerala (Kariavattom Campus), Thiruvananthapuram, for the sophisticated characterisation techniques provided for the work. S.S.S. would like to acknowledge the University Grant Commission (UGC) New Delhi, for providing Teacher Fellowship under Faculty Improvement programme (FIP).

Compliance with ethical standards

Conflict of interest The authors declare that they have no conflict of interest.

References

Boyer J-C, Cuccia LA et al (2007) Synthesis of colloidal upconverting $NaYF_4$: $Er^{3+}/Yb^{3+}$and Tm^{3+}/Yb^{3+} monodisperse nanocrystals. Nanoletters 7:847–852

Chen J, Spear SK et al (2005) Polyethylene glycol and solutions of polyethylene glycol as green reaction media. Green Chem 7: 64–82

Chen C, Li C et al. (2016) Current advances in Lanthanide-Doped Upconversion Nanostructures for Detection and Bioapplication. Adv Sci 1–26

Cooper DR, Kudinov K et al (2014) Photoluminescence of cerium fluoride and cerium-doped lanthanum fluoride nanoparticles and investigation of energy transfer to photosensitizer molecule. Phys Chem Chem Phys 16:12441–12453

DaCosta MV, Doughan S et al (2014) Lanthanide upconversion nanoparticles and applications in bioassays and bioimaging: a review. Anal Chim Acta 832:1–33

Das GK, Johnson NJ et al (2012) $NaDyF_4$ nanoparticles as T2 contrast agents for ultrahigh field magnetic resonance imaging. J Phys Chem Lett 3:524–529

Dong H, Du S-R et al (2015) Lanthanide nanoparticles: from design toward bioimaging and therapy. Chem Rev 115: 10725–10815

Gayathri S, Ghosh OSN et al (2015) Chitosan conjugation: a facile approach to enhance cell viability of LaF_3:Yb, Er upcoverting nanotransducers in human breast cancer cells. Carbohydr Polym 121:302–308

Haase M, Schafer H (2011) Upconverting nanoparticles. AngewChem Int Ed 50:5808–5829

Hu H, Chen Z et al (2008) Hydrothermal synthesis of hexagonal lanthanide-doped LaF_3 nanoplates with bright upconversion luminescence. Nanotechnology 19:375702–375711

Huang X (2016) Synthesis, multicolor tuning and emission enhancement of ultrasmall LaF_3:Yb^{3+}/ln^{3+} (Ln= Er, Tm, and Ho) upconversion nanoparticles. J Mater Sci 51:3490–3499

Jennings LE, Long NJ (2009) 'Two is better than one'—probes for dual-modality molecular imaging. Chem Commun:3511–3524

Jokerst JV, Lobovkina T et al (2011) Nanoparticle PEGylation for imaging and therapy. Nanomedicine 4:715–728

Kattel K, Park JY et al (2011) A facile synthesis, in vitro and in vivo MR studies of D-glucuronic acid-coated ultrasmall Ln_2O_3 (Ln = u, Gd, Dy, Ho, and Er) nanoparticles as a new potential MRI contrast agent. Appl Mater Interfaces 3:3325–3332

Khandpekar MM, Gaurkhede SG (2014) Redfluorescence in LaF_3:Nd^{3+}, Sm^{3+} nanocrystals grown by rapid microwave assisted synthesis: a comparative analysis of vibrational, thermal and electrical properties. J Cryst Growth 401:453–457

Lee SY, Jeon S et al (2014) Targeted multimodal imaging modalities. Adv Drug Del Rev 76:60–78

Liu C, Chen D (2007) Controlled synthesis of hexagon shaped lanthanide-doped LaF_3 nanoplates with multicolor upconversion fluorescence. J Mater Chem 17:3875–3880

Liu Y, Chen W et al (2008) X-ray luminescence of LaF_3: Tb^{3+} and LaF_3: Ce^{3+}, Tb^{3+} water-soluble nanoparticles. J Appl Phys 103:063105–063112

Mader HS, Kele P et al (2010) Upconverting luminescent nanoparticles for use in bioconjugation and bioimaging. Curr Opi Chem Biol 14:582–596

Naccache R, Yu Q et al (2015) The fluoride host: nucleation, growth, and upconversion of lanthanide-doped nanoparticles. Adv Opt Mater 3:482–509

Norek M, Peters JA (2011) MRI contrast agents based on dysprossium or holmium. Prog NMR 59:64–82

Otsuka H, Nagasaki Y et al (2003) PEGylated nanoparticles for biological and pharmaceutical applications. Adv Drug Del Rev 55:403–419

Phaomei G, Singh WR (2013) Effect of solvent on luminescence properties of re-dispersible LaF_3:Ln^{3+} (Ln^{3+} = Eu^{3+}, Dy^{3+}, Sm^{3+}, and Tb^{3+}) nanoparticles. J Rare Earths 31:347–355

Sedlmeier A, Gorris HH (2015) Surface modification and characterization of photon-upconverting nanoparticles for bioanalytical applications. Chem Soc Rev 44:1526–1560

Shameli K, Ahmad MB et al (2012) Synthesis and characterization of polyethylene glycol mediated silver nanoparticles by the green method. Int J Mol Sci 13:6639–6650

Singh AK, Kumar K et al (2013) Multi-photon assisted upconversion emission and power dependence studies in LaF_3: Er^{3+} phosphor. Spectrochim Acta Part A: Mol Biomol Spectrosc 106:236–241

Srinivasan TK, Panigrahi BS et al (2014) Gamma irradiation effect on photoluminescence from functionalized LaF_3: Ce nanoparticles. Rad Phys Chem 99:92–96

Stouwdam JW, vanVeggel FCJM (2002) Near-infrared emission of Redispersible Er^{3+}, Nd^{3+} and Ho^{3+} doped LaF_3 nanoparticles. Nanoletters 2:733–737

Vuong QL, Doorslaer SV et al (2012) Paramagnetic nanoparticles as potential MRI contrast agents: characterization, NMR relaxation, simulations and theory. Magn Reson Mater Phy 25:467–478

Wang F, Zhang Y et al (2006) Facile synthesis of water-soluble LaF_3: Ln^{3+} nanocrystals. J Mater Chem 16:1031–1034

Wu X, Chen G et al (2015) Upconversion nanoparticles: a versatile solution to multiscale biological imaging. Bioconjug Chem 26:166–175

Yu X, Liang S et al (2014) Microstructure and upconversion luminescence in Ho^{3+} and Yb^{3+} co-doped ZnO nanocrystalline powders. Opt Commun 313:90–93

Zhang Y-W, Sun X et al (2005) Single-crystalline and monodisperse LaF_3 triangular nanoplates from a single-source precursor. J Am Chem Soc 127:3260–3261

Zhang X, Hayakawa T et al (2011) Photoluminescent properties and 5D0 decay analysis of LaF_3:Eu^{3+} nanocrystals prepared by using surfactant assist. Int J Appl Ceram Technol 4:741–751

Zhou J, Liu Q et al (2015) Upconversion luminescent materials: advances and applications. Chem Rev 115:395–465

Zhu L, Meng J et al. (2007) Facile synthesis and photoluminescence of europium ion doped LaF3 nanodisks. Eur J Inorg Chem 3863–3867